Singular Integral Equation Method in the Analysis of Interaction between Rectangular Inclusions*

Nao-Aki NODA**, Qing WANG***,
Yoshitaka UEMURA** and Yuuji KAWASHIMA**

This paper deals with numerical solutions of singular integral equations in interaction problems of rectangular inclusions under various loading conditions. The body force method is used to formulate the problems as a system of singular integral equations with Cauchy-type or logarithmic-type singularities, where the unknowns are the densities of body forces distributed in infinite plates having the same elastic constants as those of the matrix and inclusions. In order to analyze the problems accurately, the unknown functions are expressed as piecewize smooth functions using two types of fundamental densities and power series, where the fundamental densities are chosen to represent the symmetric stress singularity of $1/r^{1-\lambda_1}$ and the skew-symmetric stress singularity of $1/r^{1-\lambda_2}$. Then, newly defined stress intensity factors at the end of inclusions are systematically calculated for various shapes and spacings of two rectangular inclusions in a plate subjected to longitudinal tension, transverse tension, and in-plane shear. The present method is found to be effective for accurate and efficient analysis of rectangular inclusions.

Key Words: Elasticity, Composite Material, Fracture Mechanics, Body Force Method, Stress Intensity Factor, End Effect, Interaction Effect, Singular Integral Equation, Rectangular Inclusions

1. Introduction

In previous papers[1),2)] one of the authors has considered numerical solutions of the singular integral equations of the body force method for arbitrary distributed cracks and elliptical inclusions. In these analyses a new method has been introduced, where the unknown functions are approximated by the product of "fundamental densities" and power series. The new method is found to yield rapidly converging numerical results and smooth distributions along elliptical boundaries. To express a single crack or elliptical inclusion, the exact body force densities that should be distributed in an infinite plate without crack and inclusion are available. Therefore to solve many cracks and elliptical inclusions we can use the known density as one of the "fundamental densities" effectively in the numerical solutions. The application method and the usefulness have been shown in previous papers[1),2)].

On the other hand, if we have to consider other shapes than ellipse or crack, exact body force densities are unavailable. Therefore somewhat different numerical approach seems to be necessary for the analysis. Recently, Chen and Nisitani[3),4)] have analyzed a rectangular inclusion using the body force method and discussed the magnitude of the singular stress around the corner of inclusion in detail. In their method, the unknown densities are approximated by using the fundamental densities and linear functions. To obtain the newly defined stress intensity factors (SIFs), they have examined two different methods, one of which uses the body force densities at the corner, and the other of which uses stress distribution along bisector of the corner. Because of the reason mentioned above, it can be said that to analyze rectan gular inclusions is much more difficult than to analyze elliptical inclusions and cracks. To find out an

* Received 22nd December, 1997. Japanese original: Trans. Jpn. Soc. Mech. Eng., Vol. 63, No. 612, A (1997), p. 1663-1668 (Received 18th December, 1996)
** Department of Mechanical Engineering, Kyushu Institute of Technology, 1-1 Sensui-cho, Tobata, Kitakyushu 804-8550, Japan
*** Mechanics Research Division, Department of Material Engineering, Shangdon University of Technology, Jinan, 250061, P. R. China

NII-Electronic Library Service

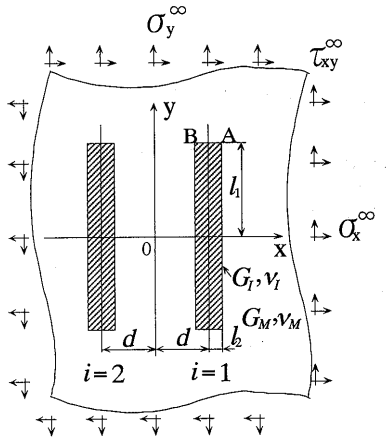

Fig. 1 Two rectangular inclusions in an infinite plate

accurate method to determine the SIFs is therefore important for rectangular inclusion problems.

In this paper, numerical solution for two rectangular inclusions as shown in Fig. 1 is considered on the singular integral equations. The interaction will be clarified with varying the shape and spacing the inclusions under three fundamental loads. The discussion will be useful for considering the mechanical strength of fiber reinforced composites.

2. Numerical Solution of Singular Integral Equations of Body Force Method

Consider two rectangular inclusions with the same configuration in an infinite plate as shown in Fig. 1. Here, l_1 and l_2 are sizes of inclusions, d is a parameter of distance, σ_x^∞, σ_y^∞ and τ_{xy}^∞ are stresses at infinity. Denote the shear modulus and Poisson's ratios of the matrix by G_M, ν_M and the inclusions by G_I, ν_I. The problem can be expressed as a system of singular integral equations (1) and (2), where the unknowns are body forces densities distributed along the imaginary boundary in two infinite plates, 'M' and 'I'. Here, the infinite plates 'M' has the same elastic constants as those of the matrix, and the infinite plate 'I' has the same elastic constants as those of the inclusions. In Eq.(1) and (2), F_{nM}, F_{tM}, F_{nI}, $F_{tI}(i=1,2)$ are unknown body force densities distributed in the normal and tangential directions along the rectangular boundary in the infinite plate 'M' or 'I'.

$$
\begin{aligned}
&-\frac{1}{2}F_{nM}(s_i)-\frac{1}{2}F_{nI}(s_i)\\
&+\sum_{k=1}^{2}\Big[\int_{L_k} h_{nn}^{F_{nM}}(r_k, s_i)F_{nM}(r_k)dr_k\\
&+\int_{L_k} h_{nn}^{F_{tM}}(r_k, s_i)F_{tM}(r_k)dr_k\\
&-\int_{L_k} h_{nn}^{F_{nI}}(r_k, s_i)F_{nI}(r_k)dr_k-\int_{L_k} h_{nn}^{F_{tI}}(r_k,\\
&s_i)F_{tI}(r_k)dr_k\Big]\\
&=-\sigma_{nM}^\infty(s_i)+\sigma_{nI}^\infty(s_i)
\end{aligned}
$$

$$
\begin{aligned}
&-\frac{1}{2}F_{tM}(s_i)-\frac{1}{2}F_{tI}(s_i)\\
&+\sum_{k=1}^{2}\Big[\int_{L_k} h_{nt}^{F_{nM}}(r_k, s_i)F_{nM}(r_k)dr_k\\
&+\int_{L_k} h_{nt}^{F_{tM}}(r_k, s_i)F_{tM}(r_k)dr_k\\
&-\int_{L_k} h_{nt}^{F_{nI}}(r_k, s_i)F_{nI}(r_k)dr_k-\int_{L_k} h_{nt}^{F_{tI}}(r_k,\\
&s_i)F_{tI}(r_k)dr_k\Big]\\
&=-\tau_{ntM}^\infty(s_i)+\tau_{ntI}^\infty(s_i)\quad (i=1,2)
\end{aligned}
\tag{1}
$$

$$
\begin{aligned}
&\sum_{k=1}^{2}\Big[\int_{L_k} h_{u}^{F_{nM}}(r_k, s_i)F_{nM}(r_k)dr_k\\
&+\int_{L_k} h_{u}^{F_{tM}}(r_k, s_i)F_{tM}(r_k)dr_k\\
&-\int_{L_k} h_{u}^{F_{nI}}(r_k, s_i)F_{nI}(r_k)dr_k-\int_{L_k} h_{u}^{F_{tI}}(r_k,\\
&s_i)F_{tI}(r_k)dr_k\Big]\\
&=-u_{M,i}^\infty+u_{I,i}^\infty\\
&\sum_{k=1}^{2}\Big[\int_{L_k} h_{v}^{F_{nM}}(r_k, s_i)F_{nM}(r_k)dr_k\\
&+\int_{L_k} h_{v}^{F_{tM}}(r_k, s_i)F_{tM}(r_k)dr_k\\
&-\int_{L_k} h_{v}^{F_{nI}}(r_k, s_i)F_{nI}(r_k)dr_k-\int_{L_k} h_{v}^{F_{tI}}(r_k,\\
&s_i)F_{tI}(r_k)dr_k\Big]\\
&=-\nu_{M,i}^\infty+\nu_{I,i}^\infty\quad (i=1,2)
\end{aligned}
\tag{2}
$$

Here, $\sum_{k=1}^{2}$ denotes the sum total about the prospective boundary of each rectangular holes and inclusions, and $\int_{L_k}$ means integrating the body forces on the boundary of the kth rectangular hole in the plate M, or the kth inclusion in the plate I. The notations $\sigma_{nM}^\infty(s_i)$ and $\tau_{ntM}^\infty(s_i)$ denote normal and shear stresses, respectively, appearing at the point s_i in plate M. As an example, the notation $h_{nn}^{F_{nM}}(r_k, s_i)$ denotes the normal stress induced at the collocation point s_i on the imaginary boundary of the ith rectangular hole when the body force with unit density F_{nM} is acting at the point r_k on the prospective boundary of the kth rectangular hole.

Equations (1) and (2) express the boundary conditions ($\sigma_{nM}-\sigma_{nI}=0$, $\tau_{ntM}-\tau_{ntI}=0$, $U_M-U_I=0$ and $V_M-V_I=0$). Here, (U_M, V_M) and (σ_{nM}, τ_{ntM}) are the displacements and tractions, respectively, on the prospective boundary of rectangular holes in the infinite plate M. On the other hand, (U_I, V_I) and (σ_{nI}, τ_{ntI}) are the displacements and tractions, respectively, on the prospective boundary of rectangular inclusions in the infinite plate I.

It is known that the body forces acting in the normal and tangential directions are expressed as two types, that is, symmetric mode I type and

NII-Electronic Library Service

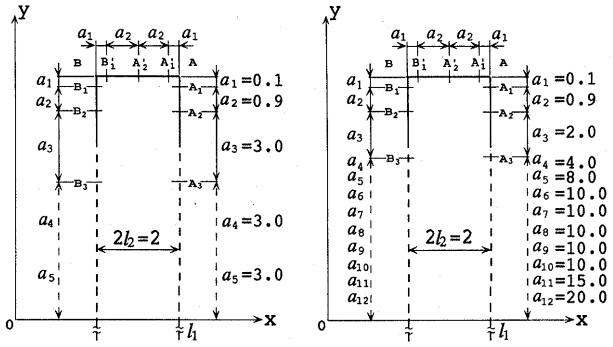

Fig. 2 Boundary division for Eqs.(3) and (4)

skew-symmetric mode II type to the bisector of the corners[3),4)]. Figure 2 illustrates boundary divisions for numerical solution of Eq.(1) and (2). In the numerical solutions for cracks and elliptical inclusions[1),2)], we do not have to divide the boundaries because the fundamental densities for a single crack or an elliptical inclusion are available. On the other hand, the boundary division is newly introduced in the author's approach because in this problem the fundamental densities are only useful near the corner.

As an example, along the region B_2-B-A-A_2 in Fig. 2 the distributed body force densities are approximated by piecewise smooth functions using power series ($W^{\mathrm{I}}_{nM}\sim W^{\mathrm{II}}_{tI}$) and two types of fundamental density functions, $r_A^{\lambda_1-1}$ and $r_A^{\lambda_2-1}$ (see (3)). In the following equations, numerical solution will be shown by taking an example for the corner A. Here, r_A is a distance measured from the corner A, and the eigenvalues λ_1 and λ_2 are given as the roots of eigenequations[3),4)]. For the corner B the solution can be represented in the same way. For the region B_2-B-A-A_2 in Fig. 2 body force distributions in the normal and tangential directions are used instead of symmetric and skew-symmetric types of distributions.

$$
\begin{aligned}
&F_{nM}(r_A)=F^{\mathrm{I}}_{nM}(r_A)+F^{\mathrm{II}}_{nM}(r_A)\\
&\quad=W^{\mathrm{I}}_{nM}(r_A)r_A^{\lambda_1-1}+W^{\mathrm{II}}_{nM}(r_A)r_A^{\lambda_2-1}\\
&F_{tM}(r_A)=F^{\mathrm{I}}_{tM}(r_A)+F^{\mathrm{II}}_{tM}(r_A)\\
&\quad=W^{\mathrm{I}}_{tM}(r_A)r_A^{\lambda_1-1}+W^{\mathrm{II}}_{tM}(r_A)r_A^{\lambda_2-1}\\
&F_{nI}(r_A)=F^{\mathrm{I}}_{nI}(r_A)+F^{\mathrm{II}}_{nI}(r_A)\\
&\quad=W^{\mathrm{I}}_{nI}(r_A)r_A^{\lambda_1-1}+W^{\mathrm{II}}_{nI}(r_A)r_A^{\lambda_2-1}\\
&F_{tI}(r_A)=F^{\mathrm{I}}_{tI}(r_A)+F^{\mathrm{II}}_{tI}(r_A)\\
&\quad=W^{\mathrm{I}}_{tI}(r_A)r_A^{\lambda_1-1}+W^{\mathrm{II}}_{tI}(r_A)r_A^{\lambda_2-1}
\end{aligned}
\qquad (3)
$$

$$
\begin{aligned}
&W^{\mathrm{I}}_{nM}(r_A)=\sum_{n=1}^{M}a_nr_A^{n-1},\quad W^{\mathrm{I}}_{tM}(r_A)=\sum_{n=1}^{M}b_nr_A^{n-1}\\
&W^{\mathrm{II}}_{nM}(r_A)=\sum_{n=1}^{M}c_nr_A^{n-1},\quad W^{\mathrm{II}}_{tM}(r_A)=\sum_{n=1}^{M}d_nr_A^{n-1}\\
&W^{\mathrm{I}}_{nI}(r_A)=\sum_{n=1}^{M}e_nr_A^{n-1},\quad W^{\mathrm{I}}_{tI}(r_A)=\sum_{n=1}^{M}f_nr_A^{n-1}\\
&W^{\mathrm{II}}_{nI}(r_A)=\sum_{n=1}^{M}g_nr_A^{n-1},\quad W^{\mathrm{II}}_{tI}(r_A)=\sum_{n=1}^{M}h_nr_A^{n-1}
\end{aligned}
\qquad (4)
$$

On the numerical method as shown in Eq.(3), (4), the singular integral equations (1), (2) are reduced to algebraic equations for the determination of the unknown coefficients $a_n\sim h_n$. These coefficients are determined from the boundary conditions at suitably chosen collocation points. The newly defined stress intensity factors K_{I,λ_1}, $F_{\mathrm{II},\lambda_2}$ for angular corners can be obtained from the values of $W^{\mathrm{I}}_n(0)$, $W^{\mathrm{II}}_n(0)$, $W^{\mathrm{I}}_t(0)$ and $W^{\mathrm{II}}_t(0)$ at the corner tip[5)].

Table 1 Convergence of F_{I,λ_1} and $F_{\mathrm{II},\lambda_2}$ at the corner B. ($l_1/l_2=10$, $l_2/d=1/3$, $G_I/G_M=10^2$, $\sigma^\infty_y=\sigma^\infty$, $\sigma^\infty_x=\tau^\infty_{xy}=0$, $\nu_I=\nu_M=0.3$, plane strain in Fig. 1)

M	F_{I,λ_1} (λ_1=0.76323491)			$F_{\mathrm{II},\lambda_2}$ (λ_2=0.62184397)		
	from $W^{\mathrm{I}}_t(0)$	from $W^{\mathrm{I}}_n(0)$	Average	from $W^{\mathrm{II}}_t(0)$	from $W^{\mathrm{II}}_n(0)$	Average
3	0.5379	0.5217	0.5298	0.7535	0.7534	0.7534
4	0.5357	0.5233	0.5293	0.7535	0.7535	0.7535
5	0.5338	0.5237	0.5287	0.7536	0.7536	0.7536
6	0.5329	0.5241	0.5286	0.7537	0.7537	0.7537

Table 2 Convergence of F_{I,λ_1} and $F_{\mathrm{II},\lambda_2}$ at the corner B. ($l_1/l_2=10^2$, $l_2/d=2/3$, $G_I/G_M=10^{-2}$, $\sigma^\infty_y=\sigma^\infty$, $\sigma^\infty_x=\tau^\infty_{xy}=0$, $\nu_I=\nu_M=0.3$, plane strain in Fig. 1)

M	F_{I,λ_1} (λ_1=0.55831618)			$F_{\mathrm{II},\lambda_2}$ (λ_2=0.91168001)		
	from $W^{\mathrm{I}}_t(0)$	from $W^{\mathrm{I}}_n(0)$	Average	from $W^{\mathrm{II}}_t(0)$	from $W^{\mathrm{II}}_n(0)$	Average
3	0.3016	0.3016	0.3016	1.7577	1.7586	1.7581
4	0.3035	0.3035	0.3035	1.7680	1.7690	1.7683
5	0.3042	0.3042	0.3042	1.7697	1.7707	1.7702
6	0.3043	0.3043	0.3043	1.7709	1.7709	1.7709

Table 3 Convergence of F_{I,λ_1} and $F_{\mathrm{II},\lambda_2}$ at the corner B. ($l_1/l_2=10^2$, $l_2/d=2/3$, $G_I/G_M=10^2$, $\sigma^\infty_y=\sigma^\infty$, $\sigma^\infty_x=\tau^\infty_{xy}=0$, $\nu_I=\nu_M=0.3$, plane strain in Fig. 1)

M	F_{I,λ_1} (λ_1=0.76323491)			$F_{\mathrm{II},\lambda_2}$ (λ_2=0.62184397)		
	from $W^{\mathrm{I}}_t(0)$	from $W^{\mathrm{I}}_n(0)$	Average	from $W^{\mathrm{II}}_t(0)$	from $W^{\mathrm{II}}_n(0)$	Average
3	0.7945	0.7575	0.7760	1.3774	1.3772	1.3773
4	0.8033	0.7740	0.7887	1.3550	1.3550	1.3550
5	0.8135	0.7881	0.8008	1.3440	1.3440	1.3440
6	0.8126	0.7909	0.8018	1.3398	1.3398	1.3398
7	0.8120	0.7916	0.8018	1.3383	1.3383	1.3383
8	0.8119	0.7916	0.8018	1.3382	1.3382	1.3382

3. Results and Discussion

In Fig. 1, the stress intensity factors K_{I,λ_1} and $K_{\mathrm{II},\lambda_2}$ defined at corners A and B are analyzed with varying geometrical parameters l_1/l_2, l_2/d, and elastic ratio G_I/G_M. In the following discussion, dimensionless stress intensity factors F_{I,λ_1} and $F_{\mathrm{II},\lambda_2}$ defined in Eq. (5), (6) are used under plane strain condition with $\nu_1=\nu_2=0.3$.

$$
\begin{aligned}
&F_{\mathrm{I},\lambda_1}=K_{\mathrm{I},\lambda_1}/\sigma^\infty\sqrt{\pi}\,l_2^{1-\lambda_1},\\
&F_{\mathrm{II},\lambda_2}=K_{\mathrm{II},\lambda_2}/\sigma^\infty\sqrt{\pi}\,l_2^{1-\lambda_2}
\end{aligned}
\qquad (5)
$$

$$
\begin{aligned}
&F_{\mathrm{I},\lambda_1}=K_{\mathrm{I},\lambda_1}/\tau^\infty\sqrt{\pi}\,l_2^{1-\lambda_1},\\
&F_{\mathrm{II},\lambda_2}=K_{\mathrm{II},\lambda_2}/\tau^\infty\sqrt{\pi}\,l_2^{1-\lambda_2}
\end{aligned}
\qquad (6)
$$

Some examples of convergence are shown in Tables 1,

NII-Electronic Library Service

Table 4 F_{I,λ_1} and F_{II,λ_2} for two rectangular inclusions at the corners A and B under various loading conditions (plane strain $\nu_I=\nu_M=0.3$)

(a) Longitudinal tension

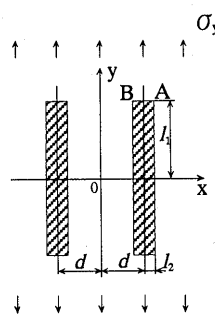

l_1/l_2	l_2/d		G_I/G_M 10^{-5}	10^{-2}	10^{-1}	10^{1}	10^{2}	10^{3}	$F_{I,\lambda_1}=K_{I,\lambda_1}/\sigma^\infty\sqrt{\pi}l_2^{1-\lambda_1}$ 10^{-5}	10^{-2}	10^{-1}	10^{1}	10^{2}	10^{3}	$F_{II,\lambda_2}=K_{II,\lambda_2}/\sigma^\infty\sqrt{\pi}l_2^{1-\lambda_2}$ 10^{-5}	10^{-2}	10^{-1}	10^{1}	10^{2}	10^{3}
10^0	0	AB	0.505	0.476	0.327	0.213	0.224	0.225	2.139	2.159	2.361	±0.493	±0.385	±0.383
	1/3	A	0.525	0.494	0.335	0.204	0.212	0.212	2.139	2.157	2.350	0.503	0.395	0.393
		B	0.555	0.522	0.355	0.211	0.220	0.222	2.124	2.141	2.332	-0.499	-0.390	-0.387
	1/2	A	0.547	0.513	0.343	0.195	0.200	0.200	2.174	2.191	2.371	0.510	0.404	0.403
		B	0.606	0.571	0.388	0.213	0.222	0.224	2.228	2.241	2.407	-0.481	-0.372	-0.368
	2/3	A	0.580	0.543	0.355	0.185	0.189	0.190	2.223	2.244	2.411	0.517	0.411	0.410
		B	0.639	0.602	0.410	0.207	0.212	0.213	2.418	2.427	2.572	-0.421	-0.313	-0.309
10^1	0	AB	0.513	0.489	0.351	0.495	0.673	0.698	1.968	1.979	2.135	±0.944	±1.018	±1.058
	1/3	A	0.583	0.550	0.379	0.466	0.593	0.587	2.017	2.030	2.189	0.856	0.903	1.007
		B	0.517	0.490	0.347	0.416	0.529	0.578	1.999	2.010	2.165	-0.810	-0.754	-0.668
	1/2	A	0.621	0.585	0.398	0.470	0.593	0.591	2.054	2.066	2.216	0.856	0.912	1.000
		B	0.466	0.444	0.323	0.372	0.456	0.503	1.976	1.990	2.147	-0.760	-0.654	-0.554
	2/3	A	0.656	0.617	0.416	0.473	0.593	0.600	2.086	2.096	2.238	0.868	0.931	1.001
		B	0.398	0.382	0.290	0.325	0.386	0.423	1.930	1.942	2.117	-0.711	-0.562	-0.480
10^2	0	AB	0.498	0.484	0.347	0.635	1.544	1.984	1.940	1.930	2.083	±1.224	±2.377	±3.064
	1/3	A	0.605	0.569	0.382	0.683	1.455	1.666	2.003	1.994	2.130	1.208	2.101	2.605
		B	0.375	0.391	0.315	0.537	1.039	1.255	1.823	1.860	2.073	-1.127	-1.679	-1.751
	1/2	A	0.632	0.591	0.398	0.695	1.469	1.678	2.024	2.003	2.145	1.233	2.185	2.697
		B	0.316	0.349	0.296	0.491	0.931	1.138	1.753	1.812	2.050	-1.086	-1.514	-1.506
	2/3	A	0.651	0.614	0.410	0.702	1.456	1.706	2.029	2.004	2.166	1.266	2.267	2.778
		B	0.255	0.304	0.272	0.434	0.802	0.993	1.682	1.771	2.027	-1.033	-1.338	-1.286

(b) Transverse tension

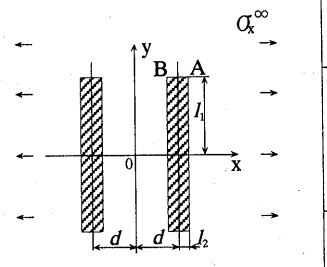

l_1/l_2	l_2/d		G_I/G_M 10^{-5}	10^{-2}	10^{-1}	10^{1}	10^{2}	10^{3}	$F_{I,\lambda_1}=K_{I,\lambda_1}/\sigma^\infty\sqrt{\pi}l_2^{1-\lambda_1}$ 10^{-5}	10^{-2}	10^{-1}	10^{1}	10^{2}	10^{3}	$F_{II,\lambda_2}=K_{II,\lambda_2}/\sigma^\infty\sqrt{\pi}l_2^{1-\lambda_2}$ 10^{-5}	10^{-2}	10^{-1}	10^{1}	10^{2}	10^{3}
10^0	0	AB	0.505	0.476	0.327	0.213	0.224	0.225	2.139	2.159	2.361	∓0.493	∓0.385	∓0.382
	1/3	A	0.496	0.468	0.324	0.224	0.237	0.239	2.025	2.046	2.265	-0.512	-0.404	-0.402
		B	0.433	0.409	0.288	0.211	0.222	0.223	1.885	1.912	2.161	0.514	0.403	0.401
	1/2	A	0.495	0.468	0.326	0.238	0.254	0.256	1.987	2.009	2.226	-0.529	-0.421	-0.421
		B	0.324	0.308	0.226	0.198	0.207	0.208	1.734	1.765	2.045	0.518	0.405	0.401
	2/3	A	0.494	0.467	0.328	0.253	0.273	0.276	1.986	2.006	2.217	-0.547	-0.441	-0.441
		B	0.212	0.203	0.159	0.179	0.188	0.189	1.702	1.736	2.036	0.485	0.371	0.365
10^1	0	AB	2.152	1.744	0.629	0.101	0.046	0.037	3.641	3.505	2.856	∓0.693	∓0.672	∓0.689
	1/3	A	2.032	1.734	0.698	0.129	0.099	0.109	3.054	2.975	2.758	-0.661	-0.637	-0.689
		B	0.771	0.698	0.393	0.113	0.079	0.052	3.491	3.348	2.886	0.642	0.560	0.502
	1/2	A	2.025	1.734	0.709	0.134	0.109	0.117	3.122	3.042	2.807	-0.666	-0.652	-0.706
		B	0.567	0.532	0.344	0.117	0.093	0.065	3.540	3.390	2.907	0.617	0.506	0.436
	2/3	A	2.017	1.733	0.714	0.141	0.119	0.123	3.195	3.111	2.848	-0.678	-0.671	-0.715
		B	0.414	0.410	0.305	0.120	0.102	0.076	3.520	3.354	2.855	0.586	0.451	0.415
10^2	0	AB	7.484	3.168	0.692	0.037	-0.333	-0.515	7.820	4.733	2.904	∓0.814	∓1.255	∓1.547
	1/3	A	7.055	3.741	0.814	0.031	-0.274	-0.356	5.837	4.304	2.960	-0.812	-1.148	-1.374
		B	1.972	1.449	0.502	0.058	-0.143	-0.238	8.763	5.502	3.027	0.777	0.953	0.969
	1/2	A	7.059	3.790	0.837	0.033	-0.270	-0.352	6.061	4.522	3.014	-0.827	-1.195	-1.426
		B	1.638	1.252	0.452	0.063	-0.113	-0.207	8.866	5.485	3.013	0.755	0.871	0.846
	2/3	A	7.063	3.818	0.845	0.038	-0.124	-0.356	6.397	4.634	3.122	-0.849	-1.243	-1.374
		B	1.306	1.067	0.409	0.069	-0.078	-0.238	8.748	5.363	2.944	0.724	0.780	0.812

(c) In-plane shear

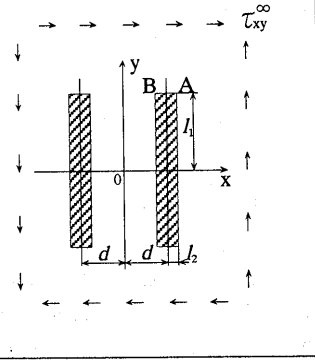

l_1/l_2	l_2/d		G_I/G_M 10^{-5}	10^{-2}	10^{-1}	10^{1}	10^{2}	10^{3}	$F_{I,\lambda_1}=K_{I,\lambda_1}/\tau^\infty\sqrt{\pi}l_2^{1-\lambda_1}$ 10^{-5}	10^{-2}	10^{-1}	10^{1}	10^{2}	10^{3}	$F_{II,\lambda_2}=K_{II,\lambda_2}/\tau^\infty\sqrt{\pi}l_2^{1-\lambda_2}$ 10^{-5}	10^{-2}	10^{-1}	10^{1}	10^{2}	10^{3}
10^0	0	AB	1.576	1.494	1.062	0.687	0.743	0.751	0.000	0.000	0.000	0.000	0.000	0.000
	1/3	A	1.696	1.602	1.115	0.674	0.731	0.740	0.143	0.138	0.106	0.015	0.015	0.015
		B	1.705	1.611	1.118	0.657	0.705	0.713	0.390	0.376	0.287	0.025	0.022	0.022
	1/2	A	1.804	1.699	1.161	0.676	0.731	0.740	0.344	0.332	0.253	0.039	0.040	0.042
		B	1.726	1.626	1.111	0.630	0.700	0.677	1.288	1.234	0.929	0.070	0.061	0.061
	2/3	A	1.895	1.782	1.201	0.682	0.739	0.747	0.550	0.531	0.411	0.070	0.070	0.076
		B	1.436	1.358	0.955	0.604	0.636	0.645	2.340	2.242	1.639	0.112	0.099	1.024
10^1	0	AB	3.923	3.547	1.894	0.743	0.809	0.819	2.514	2.494	1.520	0.262	0.372	0.424
	1/3	A	4.409	3.900	1.989	0.787	0.866	0.875	1.241	1.312	1.138	0.247	0.347	0.378
		B	1.587	1.782	1.445	0.704	0.770	0.790	3.228	2.959	1.815	0.252	0.352	0.397
	1/2	A	4.280	3.813	2.020	0.813	0.900	0.908	1.313	1.397	1.151	0.257	0.359	0.385
		B	0.731	1.354	1.281	0.659	0.721	0.745	2.062	2.444	1.783	0.222	0.315	0.353
	2/3	A	4.196	3.783	2.052	0.834	0.931	0.944	1.454	1.469	1.138	0.270	0.378	0.415
		B	0.303	1.090	1.115	0.596	0.651	0.679	1.141	2.263	1.815	0.183	0.261	0.311
10^2	0	AB	11.18	7.556	2.303	0.731	0.793	0.793	8.654	6.215	2.051	0.258	0.370	0.456
	1/3	A	11.00	8.100	2.574	0.776	0.867	0.874	4.065	4.434	1.951	0.273	0.414	0.508
		B	0.564	3.451	1.833	0.664	0.687	0.680	3.673	5.163	2.138	0.213	0.271	0.328
	1/2	A	10.97	8.242	2.664	0.794	0.888	0.899	4.131	4.745	2.036	0.279	0.428	0.535
		B	0.487	2.848	1.658	0.620	0.630	0.630	2.783	4.758	2.202	0.189	0.231	0.274
	2/3	A	10.88	8.349	2.741	0.809	0.906	0.918	4.602	4.670	1.974	0.286	0.440	0.555
		B	0.191	2.318	1.463	0.562	0.561	0.549	1.698	4.643	2.320	0.160	0.186	0.220

2, 3. The results shown in these tables are obtained using the boundary divisions shown in Fig. 2. In Tables 1, 2, 3, F_{I,λ_1} and F_{II,λ_2} values obtained from $W_n^1(0)$, $W_t^1(0)$ are indicated compared with the average values. The results have good convergency, and the difference between the results and average values are within about one percent. However, in general, the convergency is not very good when $G_I/G_M>1$, $l_1/l_2\gg 10$, and $l_2/d\to 1$. In this study the calculations are carried out when $l_1/l_2\leqq 10^2$ and $l_2/d\leqq 2/3$. Then, the

NII-Electronic Library Service

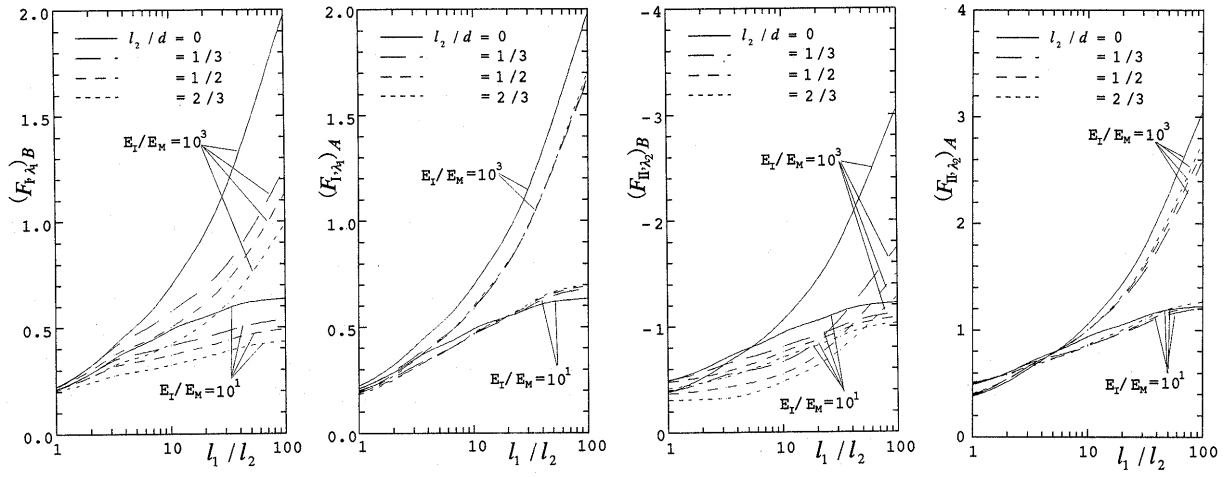

Fig. 3 F_{I,λ_1}, F_{II,λ_2} vs. l_1/l_2 relations for two rectangular inclusions at the corners A and B in Fig. 1 ($\sigma_y^\infty=\sigma^\infty$, $\sigma_x^\infty=0$, $\tau_{xy}^\infty=0$, Plane strain $\nu_I=\nu_M=0.3$)

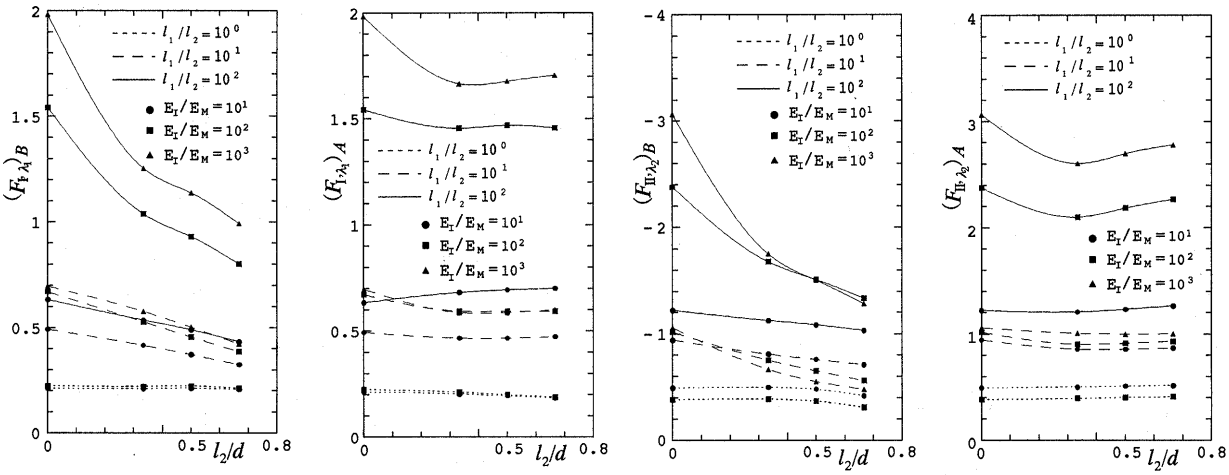

Fig. 4 F_{I,λ_1}, F_{II,λ_2} vs. l_2/d relations for two rectangular inclusions at the corners A and B in Fig. 1 ($\sigma_y^\infty=\sigma^\infty$, $\sigma_x^\infty=0$, $\tau_{xy}^\infty=0$, Plane strain $\nu_I=\nu_M=0.3$)

values obtained from $W_n^1(0)$, $W_t^1(0)$ and the average value coincide with each other in about three digits when M=6 or 8.

Table 4 shows the intensity factors F_{I,λ_1} and F_{II,λ_2} at the corners A and B under three fundamental loads. Figure 3 shows F_{I,λ_1} (or F_{II,λ_2}) vs. l_1/l_2 relation and Fig. 4 shows F_{I,λ_1} (or F_{II,λ_2}) vs. l_2/d relation under longitudinal tension. From those tables and figures, it is found that the interaction is large at the corner B and small at the corner A regardless of loading conditions. For example, when $G_I/G_M=10^3$, $l_1/l_2=10^2$, and $l_2/d=2/3$ under longitudinal tension, F_{I,λ_1} value is about 50% of the value of a single inclusion at the corner B and about 85% of the one at the corner A.

Figures 6 and 7 show the results under uniaxial tension with varying tensile direction α from 0° (x-direction) to 180° ($-x$-direction) as shown in Fig. 5. In these figures, the interaction appears most largely at nearly $\alpha=90°$ (y-direction) when $G_I/G_M>1$. On the other hand, when $G_I/G_M<1$ the interaction appears

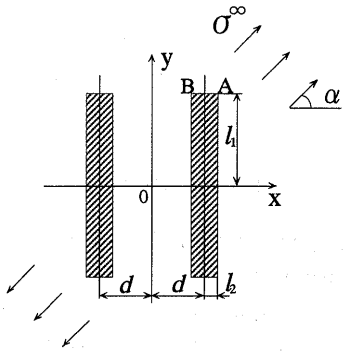

Fig. 5 Two rectangular inclusions in a plate subjected to uniaxial tension in α direction

most largely at nearly $\alpha=135°$. When $G_I/G_M<1$, the effect of spacing is small in the range from $l_2/d=1/3$ to $l_2/d=2/3$; however, the difference is large between a single inclusion ($l_2/d=0$) and double inclusions ($l_2/d=1/3\sim2/3$).

NII-Electronic Library Service

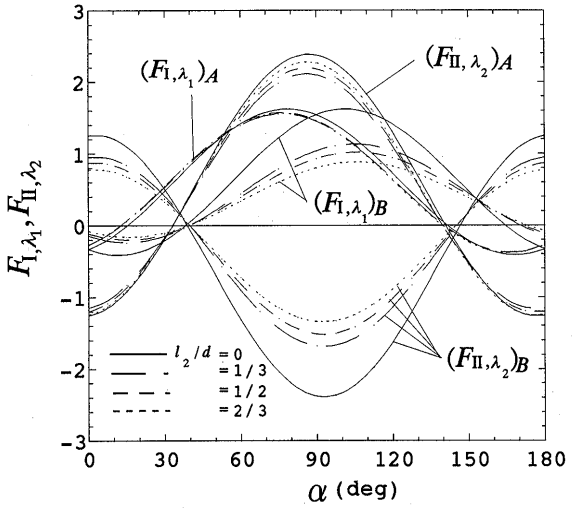

Fig. 6 F_{I,λ_1}, F_{II,λ_2} vs. α relations at the corners A and B in Fig. 5 ($l_1/l_2=10^2$, $G_I/G_M=10^2$, Plane strain, $\nu_I=\nu_M=0.3$)

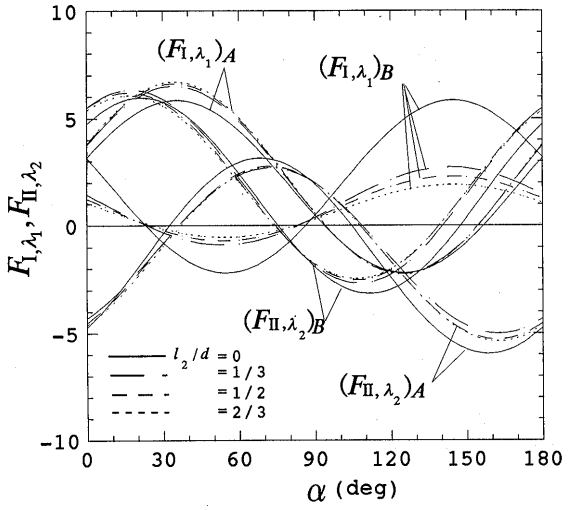

Fig. 7 F_{I,λ_1}, F_{II,λ_2} vs. α relations at the corners A and B in Fig. 5 ($l_1/l_2=10^2$, $G_I/G_M=10^{-2}$, Plane strain, $\nu_I=\nu_M=0.3$)

4. Conclusions

In this paper, numerical solution of the singular integral equation and interaction effect were considered in two rectangular inclusions as shown in Fig. 1. Newly defined stress intensity factors at the corners of inclusions were discussed under various geometrical and loading conditions. The conclusions can be made as follows.

(1) In the numerical solution of the singular integral equations of the body force method, the unknown body force densities are approximated by a piecewise smooth functions using power series and two types of fundamental density functions, $r_A^{\lambda_1-1}$ and $r_A^{\lambda_2-1}$ (see Eq. (3), (4) and Fig. 2). The calculation shows that the present method yields rapidly converging results for the wide range of geometrical and elastic conditions. The difference between the results obtained from different functions and the average values are within about one percent.

(2) The interaction is large at the inside corner B and small at the outside corner A regardless of loading conditions. For example, when $G_I/G_M=10^3$, $l_1/l_2=10^2$, and $l_2/d=2/3$ under longitudinal tension, F_{I,λ_1} value is about 50% of the value of a single inclusion at the corner B and about 85% of the one at the corner A.

(3) In the uniaxial tension in α direction as shown in Fig. 5, the interaction appears most largely at nearly $\alpha=90°$ (y-direction) when $G_I/G_M>1$. On the other hand, when $G_I/G_M<1$ the interaction appears most largely at nearly $\alpha=135°$. When $G_I/G_M<1$, the effect of spacing is small in the range from $l_2/d=1/3$ to $l_2/d=2/3$; however, the difference is large between a single inclusion ($l_2/d=0$) and double inclusions ($l_2/d=1/3\sim2/3$).

Acknowledgement

This research was supported by Kyushu Institute of Technology Fellowship for Foreign Researchers.

References

(1) Noda, N.-A. and Matsuo, T., Singular Integral Equation Method in the Analysis of Interaction between Cracks and Defects, Fracture Mechanics; 25th Volume. ASTM STP 1220, F. Erdogan, Ed. (1995), p. 591-606, American Society for Testing and Materials, Philadelphia.

(2) Noda, N.-A., Fukuda, K. and Matsuo, T., Analysis of Interaction among Arbitrary Distributed Elliptical Inclusions, Journal of the Japan Society of Material Science, (in Japanese), Vol. 45, No. 12 (1996), p. 1334-1339.

(3) Chen, D.H. and Nisitani, H., Analysis of Singular Stress at the Fiber End (First Report, Theory), Trans. Jpn. Soc. Mech. Eng., (in Japanese), Vol. 58, No. 554, A (1992), p. 1834-1838.

(4) Chen, D.H. and Nisitani, H., Analysis of Singular Stress at the Fiber End (Second Report, Results and Discussion), Trans. Jpn. Soc. Mech. Eng., (in Japanese), Vol. 58, No. 554, A (1992), p. 2153-2158.

(5) Noda, N.-A., Kawashima, Y., Moriyama, S. and Oda, K., Interaction of Newly Defined Stress Intensity Factors for Angular Corners in a Row of Diamond-Shaped Inclusions, International Journal of Fracture, Vol. 82 (1996), p. 267-295.

NII-Electronic Library Service